Analytical model for determining effective stiffness and mechanical behavior of polymer matrix composite laminates using continuum damage mechanics

Okabe, Tomonaga
Department of Aerospace Engineering, Tohoku University

Onodera, Sota
Department of Aerospace Engineering, Tohoku University

出版情報：International Journal of Damage Mechanics. 29 (10), pp.1512-1542, 2020-07-26. SAGE Publications
バージョン：

Journal Title
XX(X):2–34

DOI: 10.1177/ToBeAssigned
www.sagepub.com/
SAGE

Analytical model for determining effective stiffness and mechanical behavior of polymer matrix composite laminates using continuum damage mechanics

Sota Onodera[1] and Tomonaga Okabe[1,2]

Abstract

The present paper proposes a new analytical model for predicting the effective stiffness of composite laminates with fiber breaks and transverse cracks. The model is based on continuum damage mechanics and the classical laminate theory. We derived damage variables describing stiffness reduction due to fiber breaks and its maximum value during ultimate tensile failure from the global load-sharing model. Furthermore, a simplified analytical model is presented for obtaining two damage variables for a cracked ply subjected to transverse tensile loading or in-plane shear loading. This model was developed assuming that the displacement field of the longitudinal direction can be expressed in the form of a quadric function by loosening the boundary condition for the governing differential equation. For verifying the developed model, the elastic constants of damaged composite laminates were predicted for cross-ply and angle-ply laminates and compared with finite element analysis results. As for the appropriate expression of the effective elastic stiffness matrix of the damaged ply, we verified four types of effective compliance/stiffness matrices including the Murakami, Yoshimura, Li and Maimí models. We found the Maimí model to be the most appropriate among these four models. Moreover, we successfully simplified the expressions for damage variables in the complicated infinite series obtained in our previous study. We also proved that this could contribute toward improving the accuracy of our analysis. After verifying the present model, the stress-strain response and failure strength of carbon- or glass- fiber-reinforced plastic cross-ply laminates were predicted using Maimí's compliance model and the simplified damage variables.

Keywords
transverse crack, continuum damage mechanics, damage variable, composite laminate, polymer matrix composite

Introduction

The application scope of advanced composite materials is increasing due to their superior mechanical properties like high specific modulus and strength. The specific modulus plays an important role in real structures, but the specific strength of these materials has not been effectively utilized in real applications owing to the incapability of failure analysis. The reason why effective designs considering the high specific strength are not yet developed is that structural designs are developed using the strain criterion based on initial ply failure. When load is applied to composite structures, matrix cracks are generated in the transverse ply. However, if the applied strain level is low, these cracks do not cause secondary damage and affect the reduction of stiffness. Furthermore, if the applied strain reaches a certain level, the damage migrates from the ply cracks, leading to catastrophic damage phenomena like delamination and fiber breakage. Thus, similar to metals, if designers consider the initial damage and users can predict the progress of the damage, the structural weight can be reduced. Therefore, damage tolerance designing is the next step for expanding the application scope of composite structures.

Designers need to analyze the stiffness reduction in composite structures owing to transverse cracks accurately. Transverse cracks occurring in cross-ply laminates have been studied since the 1970s.[1–6] Initially, there were many stress analysis studies performed using the shear-lag model, which was developed to analyze the stress profile around discontinuous fibers.[7] Using the shear-lag model, the damage progress could be predicted using the stress criterion and/or energy criterion. Specifically, the onset of transverse cracks from the viewpoint of micromechanics was analyzed. In the 1980s, the shear-lag model was improved.[8,9] Finite element analysis (FEA)[10] and the minimum energy principle model[11–13] utilizing variation methods were proposed to analyze the stress field around the transverse cracks. These models enable us to calculate the stress field around the transverse cracks in cross-ply laminates very accurately.

In addition to the above approaches, continuous damage mechanics (CDM) models[14–16] were developed simultaneously. CDM models are divided into the following two types: the first one involves the effective elastic stiffness or compliance matrix

[1]Department of Aerospace Engineering, Tohoku University, 6-6-01, Aramaki Aza Aoba, Aoba-ku, Sendai, Miyagi, Japan, 980-8579
[2]Department of Materials Science and Engineering, University of Washington, Box 352120 Seattle, WA, U.S.A., 98195-2120

Corresponding author:
Sota Onodera, Department of Aerospace Engineering, Tohoku University, 6-6-01, Aramaki Aza Aoba, Aoba-ku, Sendai, Miyagi, Japan, 980-8579
Email: sonodera@plum.mech.tohoku.ac.jp

utilizing the damage tensor derived from the thermomechanical relationship; while the other one calculates the inelastic strain with internal state variables so that the average stress of the laminate can be estimated. Both models are fitted with the classical laminate theory (CLT) because the detailed stress distribution in the laminate is unnecessary and the damaged ply is homogenized. Therefore, arbitrary laminates other than cross-ply laminates can be analyzed easily. On the contrary, problems regarding the objective determination of damage tensor and internal state variables must be addressed.

In the 1990s, McCartney[17] presented an accurate anisotropic elastic solution for cross-ply laminates, satisfying both the equilibrium and compatible equation. Pagano et al.[18] proposed an accurate solution based on cylindrical bending. Moreover, several researchers analyzed the delamination migrating from the matrix crack from the view point of energy balance.[19,20] Xia et al.[21] used the McCartney model to analyze damage progress in ceramic-matrix cross-ply laminates. Furthermore, using CDM, Gudmundson and Zang[22] extended the two-dimensional model of Dvorak et al.[23,24] which is applicable to an isotropic body, to obtain a three dimensional model with the generalized laminate theory for analyzing three-dimensional laminates. As stated above, CDM can be applied to angle-ply laminates. Gudmundson and Zang applied the model to study stiffness reduction in angle-ply laminates. Kobayashi et al.[25] used the Gudmundson and Zang model to predict the damage progress in quasi-isotropic carbon-fiber-reinforced plastic (CFRP) laminates. After the 2000s, several researchers[26–28] continued to develop models for analyzing arbitrary laminates other than cross-ply laminates. However, the derived formulations are extremely complicated for ordinary people to use them easily.

Recently, we derived the analytical form of the damage tensor with transverse crack density by solving the Laplace equation for the displacement fields under the generalized plane strain condition.[29] The laminate stiffness can be estimated with the obtained damage tensor through the CLT and CDM model proposed by Murakami and his colleagues.[30,31] We have also proved that the estimated stiffness agrees with the finite element calculations and experimental results.[14] This approach is extended to a three-dimensional model[32] using a sophisticated model proposed by Li et al.[33] However, the effective compliance matrix proposed by Murakami and his colleagues is asymmetric. This asymmetry of the compliance matrix was also observed in the study done by Lee et al.[13] Furthermore, because the damage tensor is derived by solving the Laplace equation, it is written as a complicated infinite series.[29]

The fiber breakage generally causes nonlinearity in the stress-strain curves when the applied strain is large. It is well known that Rosen[34] originally studied the stress transfer length around fiber breaks as well as the unidirectional composite failure strength and applied to glass-epoxy monolayer specimens. Analytical models considering fiber breakage have been mainly developed in the field of ceramic matrix composites (CMCs) since the late 1980's. This is because a stress concentration due to a fiber break can almost be neglected, so that the global load sharing model (GLS), wherein the load shed by a broken fiber is shared by all intact fibers, can be directly applied to the experiments. Curtin[35] presents a famous theory to predict the ultimate tensile strength of the unidirectional composites assuming the GLS model. Neumeister[36] developed an approximate solution of the stress-strain curve and strength of the composite, and

compared to a numerical result based on the fiber fragmentation theory formulated by Curtin.[37] Hui et al.[38] derived an explicit closed form solution of the evolution of fiber fragments and applied to estimate the strength of unidirectional composite materials. In general, the GLS models give a larger strength than the local load-sharing (LLS) model that considers local stress concentrations caused by fiber breaks.[39] However, the GLS models are theoretically easy to handle. Therefore, it is suitable to utilize the GLS models to analytically formulate the damage tensor.

This study developed an appropriate expression for the effective stiffness matrix of damaged composite laminates and derived simplified expressions for the damage tensor with the fiber breakage and transverse crack density. Damage variable for fiber breakage was formulated using the GLS model for unidirectional fiber-reinforced composites. An approximate simplified expression for the damage tensor with transverse crack density was obtained from the Laplace equation, assuming the quadratic function. For validating the present model, the obtained damage tensor was substituted into CDM and CLT models, and the elastic constants of damaged composite laminates were then predicted for cross-ply and angle-ply laminates. As for the appropriate expression for the effective compliance/stiffness matrix of a damaged ply, we verified four types of damage matrices including the Murakami[30,31], Yoshimura[40], Li[33] and Maimí models.[41] We determined that the Maimí model was the most appropriate among these four models. Moreover, we succeeded in simplifying the expression for damage variables with complicated infinite series obtained in our previous study. We also proved that this could contribute toward the improving the analysis accuracy. Further, we determined the nonlinear stress-strain response and ultimate tensile strength of CFRP and glass-fiber-reinforced-plastic (GFRP) cross-ply laminates. We employed the Maimí model and simplified damage variables proposed in this study when calculating the stress-strain response. The ultimate tensile strength of CFRP cross-ply laminates was predicted based on a strain-based fiber failure criterion[27] because fiber fracture in CFRP laminates often occurs at the point of laminate failure. For GFRP laminates, the stiffness reduction due to multiple-fiber fragmentation in 0° plies and the subsequent final laminate failure were determined using the GLS model.

Model formulation

Effective elastic compliance/stiffness matrix of damaged ply

Four models for the elastic compliance matrix of a damaged composite ply under the plane stress condition are introduced here and their characteristics are explained.

Model 1: Murakami model Murakami published a sophisticated book[30] introducing CDM and proposed a compliance matrix for damaged composite plies with his

colleagues.[31] They used the strain equivalent principle to obtain the following stress-strain relationship:

$$\begin{pmatrix} \varepsilon_{11} \\ \varepsilon_{22} \\ 2\varepsilon_{12} \end{pmatrix} = \begin{pmatrix} \frac{1}{(1-d_{11})E_1} & -\frac{\nu_{12}}{(1-d_{22})E_1} & 0 \\ -\frac{\nu_{12}}{(1-d_{11})E_1} & \frac{1}{(1-d_{22})E_2} & 0 \\ 0 & 0 & \frac{1}{2}\left(\frac{1}{1-d_{11}} + \frac{1}{1-d_{22}}\right)\frac{1}{G_{12}} \end{pmatrix} \begin{pmatrix} \sigma_{11} \\ \sigma_{22} \\ \sigma_{12} \end{pmatrix}. \quad (1)$$

E_i is the Young's modulus, G_{ij} is the shear modulus, ν_{ij} is the Poisson's ratio, ε_{ij} is the strain tensor, σ_{ij} is the stress tensor, and d_{ij} is the damage variable. In Eq. (1), subscripts 1 and 2 denote the fiber direction and the in-plane transverse direction respectively. In our previous study, we found that this matrix is effective for obtaining the elastic constants of damaged composite laminates if the appropriate damage tensor is used. However, the compliance matrix in Eq. (1) is obviously asymmetric and this violates the existence of the strain energy function. Moreover, this form cannot be directly entered into the numerical simulation code as in FEA. As stated above, this asymmetry of the compliance matrix was also observed in the work of Lee.[13]

Model 2: Yoshimura model Yoshimura et al.[40] proposed the concept of the stress equivalent principle to overcome the difficulty of the asymmetry of the compliance matrix. The stress-strain relation can be written as:

$$\begin{pmatrix} \sigma_{11} \\ \sigma_{22} \\ \sigma_{12} \end{pmatrix} = \begin{pmatrix} B_{11} & B_{12} & 0 \\ & B_{22} & 0 \\ \text{sym.} & & B_{33} \end{pmatrix} \begin{pmatrix} \varepsilon_{11} \\ \varepsilon_{22} \\ 2\varepsilon_{12} \end{pmatrix}, \quad (2)$$

where

$$B_{11} = \frac{(1-d_{11})E_1}{1-\nu_{12}\nu_{21}} - \frac{d_{11}^2}{4}\frac{\nu_{12}\nu_{21}(1+\nu_{23})E_1}{\Delta(1-\nu_{12}\nu_{21})}, \quad (3)$$

$$B_{12} = \frac{\left(1-\frac{d_{11}+d_{22}}{2}\right)\nu_{12}E_2}{1-\nu_{12}\nu_{21}} - \frac{d_{11}d_{22}}{4}\frac{\nu_{12}(\nu_{23}+\nu_{12}\nu_{21})E_2}{\Delta(1-\nu_{12}\nu_{21})}, \quad (4)$$

$$B_{22} = \frac{(1-d_{22})E_2}{1-\nu_{12}\nu_{21}} - \frac{d_{22}^2}{4}\frac{(\nu_{23}+\nu_{12}\nu_{21})^2E_2}{\Delta(1+\nu_{23})(1-\nu_{12}\nu_{21})}, \quad (5)$$

$$B_{33} = \left(1-\frac{d_{11}+d_{22}}{2}\right)G_{12}, \quad (6)$$

$$\Delta = 1-\nu_{23}-2\nu_{12}\nu_{21}. \quad (7)$$

In this case, the stiffness matrix is obviously symmetric. This effective stiffness matrix has already been inserted into the ABAQUS user subroutine to simulate the high-velocity impact problem. The simulation results roughly reproduced the damage progress observed experimentally, but the simulation underestimated the extent of damage compared to the experiments. Moreover, the degradation coefficient of shear modulus does not have any physical meaning. These points are discussed later when comparing the four models explained in this section.

Model 3: Li model Li et al.[33] formulated the three-dimensional effective stiffness matrix for a ply with transverse cracking assuming a small damage. The two-dimensional effective stiffness matrix can be written as:

$$\begin{pmatrix}\sigma_{11}\\ \sigma_{22}\\ \sigma_{12}\end{pmatrix} = \begin{pmatrix} C_{11}-\frac{C_{13}^2}{C_{33}} & C_{12}-\frac{C_{13}C_{23}}{C_{33}} & 0 \\ & C_{22}-\frac{C_{23}^2}{C_{33}} & 0 \\ \text{sym.} & & C_{66}\end{pmatrix}\begin{pmatrix}\varepsilon_{11}\\ \varepsilon_{22}\\ 2\varepsilon_{12}\end{pmatrix}, \tag{8}$$

where

$$C_{11} = \frac{1-\nu_{23}}{\Delta}E_1 - \omega\frac{E_1\nu_{12}\nu_{21}}{\Delta^2}, \tag{9}$$

$$C_{12} = \frac{\nu_{12}}{\Delta}E_2 - \omega\frac{E_2\nu_{12}(1-\nu_{12}\nu_{21})}{(1+\nu_{23})\Delta^2}, \tag{10}$$

$$C_{13} = \frac{\nu_{12}}{\Delta}E_2 - \omega\frac{E_2\nu_{12}(\nu_{23}+\nu_{12}\nu_{21})}{(1+\nu_{23})\Delta^2}, \tag{11}$$

$$C_{22} = \frac{1-\nu_{12}\nu_{21}}{(1+\nu_{23})\Delta}E_2 - \omega\frac{E_2(1-\nu_{12}\nu_{21})^2}{(1+\nu_{23})^2\Delta^2}, \tag{12}$$

$$C_{23} = \frac{\nu_{23}+\nu_{12}\nu_{21}}{(1+\nu_{23})\Delta}E_2 - \omega\frac{E_2(1-\nu_{12}\nu_{21})(\nu_{23}+\nu_{12}\nu_{21})}{(1+\nu_{23})^2\Delta^2}, \tag{13}$$

$$C_{33} = \frac{1-\nu_{12}\nu_{21}}{(1+\nu_{23})\Delta}E_2 - \omega\frac{E_2(\nu_{23}+\nu_{12}\nu_{21})^2}{(1+\nu_{23})^2\Delta^2}, \tag{14}$$

$$C_{66} = G_{12} - \xi\omega G_{12}. \tag{15}$$

Here, ω is the damage parameter related to tensile damage and ξ is the constant damage parameter related to shear damage. ω and ξ can be expressed as follows:[32]

$$\omega = 1 - \frac{E_2^d}{E_2} = d_{22}, \tag{16}$$

$$\xi = \frac{1}{\omega}\left(1 - \frac{G_{12}^d}{G_{12}}\right) \approx \frac{1}{\lambda}. \tag{17}$$

Here, superscript d denotes the property of the damaged ply and λ is the material constant described later. Onodera and Okabe[32] utilized this effective stiffness for predicting the stiffness reduction and steady-state cracking of laminates with ply cracking. The proposed CDM model agrees with the experimental and numerical results.[32] However, the damage parameter ω and transverse crack density have upper limits because a small damage was assumed.

Model 4: Maimí model Maimí et al.[41] proposed the complementary free energy function and thermodynamically derived the effective compliance matrix as follows:

$$\begin{pmatrix}\varepsilon_{11}\\ \varepsilon_{22}\\ 2\varepsilon_{12}\end{pmatrix} = \begin{pmatrix} \frac{1}{(1-d_{11})E_1} & -\frac{\nu_{12}}{E_1} & 0 \\ & \frac{1}{(1-d_{22})E_2} & 0 \\ \text{sym.} & & \frac{1}{(1-d_{12})G_{12}}\end{pmatrix}\begin{pmatrix}\sigma_{11}\\ \sigma_{22}\\ \sigma_{12}\end{pmatrix}. \tag{18}$$

The effective compliance matrix in this case is also explicitly symmetric. However, this case needs an additional damage variable d_{12} for evaluating the shear stiffness reduction due to transverse cracks or fiber breaks. For the ply with transverse cracks, this parameter is derived from the displacement field of the damaged ply in this study. For the ply with fiber breaks, d_{12} can be approximated as follows:[30]

$$\frac{1}{1-d_{12}} = \frac{1}{2}\left(\frac{1}{1-d_{11}} + 1\right). \tag{19}$$

The approximate relation of Eq. (19) was used when considering the ply with fiber breaks.

Damage variables

Damage variable d_{11} for multi-fiber fragmentation An analytical expression for d_{11} was developed by employing Curtin's GLS model[35] considering the ultimate tensile strength of unidirectional fiber-reinforced composites. Now, we consider the mechanical equilibrium on an arbitrary cross section in a unidirectional fiber-reinforced composite with broken fibers. Utilizing the shear-lag model, the slip length l_f can be described as

$$l_f = \frac{rT}{2\tau}, \tag{20}$$

where T is the far-field axial fiber stress, τ is the fiber/matrix interfacial sliding stress, and r is the fiber radius. If fiber breaks occur equally within the range $\pm l_f$, then the average stress carried by the broken fibers in the selected plane is half of that carried by the unbroken fibers. The stress carried by the broken and unbroken fibers in the selected plane can be described as

$$\overline{\sigma}_f = T\{1 - P_f(T, 2l_f)\} + \frac{T}{2}P_f(T, 2l_f). \tag{21}$$

Here, the first term on the right-hand side represents the load carried by the unbroken fiber with the fraction $1 - P_f(T, 2l_f)$ and the second term is the average load carried by the broken fibers, whose fraction is $P_f(T, 2l_f)$. It is well known that the probability $P_f(T, 2l_f)$ of the fiber failure with applied stress T and length $2l_f$ can be simplified as

$$P_f(T, 2l_f) \approx \frac{2l_f}{L_0}\left(\frac{T}{\sigma_0}\right)^m = \left(\frac{T}{\sigma_c}\right)^{m+1} \quad \text{if} \quad \frac{2l_f}{L_0}\left(\frac{T}{\sigma_0}\right)^m \ll 1, \tag{22}$$

where m is the Weibull modulus and σ_0 is the mean strength at gauge length L_0. σ_c is the characteristic strength defined as follows:

$$\sigma_c = \left(\frac{\sigma_0 \tau L_0}{r}\right)^{1/(m+1)}. \tag{23}$$

In the selected cross section, the following mechanical equilibrium condition must be satisfied:

$$\sigma_1 = f\overline{\sigma}_f, \tag{24}$$

σ_1 is the stress applied on the unidirectional composite along the fiber direction and f is the fiber volume fraction. Using the Voigt model for representing the Young's modulus of composite, the unidirectional axial composite stress σ_1, axial fiber stress T, and unidirectional Yong's modulus E_1 are expressed as

$$\sigma_1 = (1 - d_{11})E_1\varepsilon_1, \tag{25}$$

$$T = E_f\varepsilon_1, \tag{26}$$

$$E_1 = fE_f + (1 - f)E_m \approx fE_f. \tag{27}$$

Here, ε_1 is the unidirectional composite strain, E_f is the fiber axial modulus, and E_m is the matrix modulus. We neglected the term $(1 - f)E_m$ in Eq. (27) because $E_f \gg E_m$ is approximately satisfied in the case of polymer matrix composites. Using Eqs. (21), (22) and (25) - (27) in Eq. (24), the damage variable was simply derived as

$$d_{11} = \frac{1}{2}\left(\frac{T}{\sigma_c}\right)^{m+1}. \tag{28}$$

The remaining unknown variable is the far-field fiber axial stress T. Substituting Eqs. (21) and (22) into Eq. (24), the following nonlinear equation for T was obtained.

$$\sigma_1 = fT\left(1 - \frac{1}{2}\left(\frac{T}{\sigma_c}\right)^{m+1}\right) \tag{29}$$

Stress T at applied load σ_1 was numerically obtained by solving the above nonlinear equation. When a cross-ply laminate having 0° plies with volume fraction V_1 and the 90° plies with volume fraction V_2 is considered, the applied axial laminate stress $\overline{\sigma}_L$ can be described using the rule of mixture as follows:

$$\overline{\sigma}_L = V_1\sigma_1 + V_2\sigma_2 \approx V_1\sigma_1, \tag{30}$$

σ_1 is the 0° ply stress and σ_2 is the 90° ply stress. We decided to neglect the second term on the right-hand side in Eq. (30). This is because fiber breaks in the 0° ply may start after the saturation of transverse cracks and the 90° plies have very small load-bearing capacity during saturation of transverse cracks. Using Eq. (30) in Eq. (29), the nonlinear expression for stress T is rewritten as

$$\frac{\overline{\sigma}_L}{V_1} = fT\left(1 - \frac{1}{2}\left(\frac{T}{\sigma_c}\right)^{m+1}\right). \tag{31}$$

The ultimate tensile strength of cross-ply laminates can be derived using Eq. (31). The ultimate failure condition of composite laminates is described by the following equation:

$$\frac{d\overline{\sigma}_L}{dT} = 0. \tag{32}$$

The maximum far-field fiber stress $T_{\max}$ and ultimate tensile strength $\overline{\sigma}_L^{\mathrm{ULT}}$ of cross-ply laminates were simply obtained by substituting Eq. (31) into Eq. (32).

$$T_{\max} = \left(\frac{2}{m+2}\right)^{1/(m+1)} \sigma_c \tag{33}$$

$$\overline{\sigma}_L^{\mathrm{ULT}} = V_1 f \sigma_c \left(\frac{2}{m+2}\right)^{1/(m+1)} \frac{m+1}{m+2} \tag{34}$$

The maximum value of damage variable d_{11} was obtained using Eq. (33) in Eq. (28).

$$d_{11}^{\max} = \frac{1}{m+2} \tag{35}$$

d_{11} increased to its maximum value in Eq. (35) under the ultimate tensile failure condition. In this study, the far-field stress T was calculated using the Newton method to solve the nonlinear equation (Eq.(31)) at a given laminate tensile stress $\overline{\sigma}_L$ until the ultimate tensile failure condition in Eq. (32) was satisfied. d_{11} was obtained using the calculated stress T in Eq. (28).

Damage variable d_{22} associated with transverse cracking In any of the effective stiffness/compliance models stated above, d_{22} is necessary to evaluate the compliance/stiffness matrix of the damaged ply. The governing equation (i.e., Laplace equation) of the corresponding problem was derived. The simplified solution of the equation obtained assuming that the displacement field in the longitudinal direction can be expressed as a quadric function. Further, the boundary condition for the governing equation was loosened.

As shown in Fig. 1, the solved problem is the displacement field for the damaged transverse ply including periodic matrix cracks having an interval of $2l$. These matrix cracks fully propagate in the z direction and reach the interface. The longitudinal strain of the neighboring ply is assumed to be uniform and unaffected by these cracks. Considering the symmetry of the problem, only the first quadrant in the xy plane was addressed. The plane strain condition was assumed, and the constitutive relations are given by

$$\varepsilon_{xx}(x,y) = \frac{\partial u(x,y)}{\partial x} = C_1\sigma_{xx}(x,y) - C_2\sigma_{yy}(x,y), \tag{36}$$

$$\varepsilon_{yy}(x,y) = \frac{\partial v(x,y)}{\partial y} = C_1\sigma_{yy}(x,y) - C_2\sigma_{xx}(x,y), \tag{37}$$

$$\gamma_{xy}(x,y) = \frac{\sigma_{xy}(x,y)}{G_{23}} = \frac{\partial v(x,y)}{\partial x} + \frac{\partial u(x,y)}{\partial y} \approx \frac{\partial v(x,y)}{\partial x}. \tag{38}$$

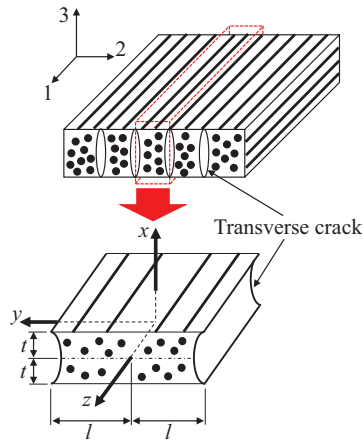

Figure 1. Representative volume element in a cracked ply with transverse crack spacing $2l$ and ply thickness $2t$. $(1, 2, 3)$ is the material coordinate system, and (x, y, z) is the representative volume element coordinate system.

Here, u and v are the displacements along the x and y directions respectively. C_1 and C_2 are given by

$$C_1 = \frac{1 - \nu_{12}\nu_{21}}{E_2}, \quad C_2 = \frac{\nu_{23} + \nu_{12}\nu_{21}}{E_2}. \tag{39}$$

We assumed that $\partial u/\partial y$ was negligible in Eq. (38) so that the compatible condition of the strain tensor was not satisfied. To obtain the governing equation for displacement v, the following relationship was introduced:

$$\varepsilon_{xx}(x, y) = a\varepsilon_{yy}(x, y), \tag{40}$$

where a is the effective Poisson's ratio derived from the equilibrium equation. Substituting Eq. (40) into Eqs. (36) and (37), we obtained the stress with displacement v as follows:

$$\sigma_{xx}(x, y) = \frac{aC_1 + C_2}{C_1^2 - C_2^2} \frac{\partial v(x, y)}{\partial y}, \tag{41}$$

$$\sigma_{yy}(x, y) = \frac{C_1 + aC_2}{C_1^2 - C_2^2} \frac{\partial v(x, y)}{\partial y}. \tag{42}$$

These stresses satisfy the following two-dimensional equilibrium equations:

$$\frac{\partial \sigma_{xx}}{\partial x} + \frac{\partial \sigma_{xy}}{\partial y} = 0, \tag{43}$$

$$\frac{\partial \sigma_{xy}}{\partial x} + \frac{\partial \sigma_{yy}}{\partial y} = 0. \tag{44}$$

Substituting Eqs. (38) and (41) into Eqs. (43) and removing the trivial case (i.e., $\partial^2 v/\partial x \partial y \neq 0$), a was calculated as

$$\begin{aligned} a &= -\frac{C_2 + G_{23}(C_1^2 - C_2^2)}{C_1} \\ &= -\frac{E_2(\nu_{23} + \nu_{12}\nu_{21}) + G_{23}\{(1 - \nu_{12}\nu_{21})^2 - (\nu_{23} + \nu_{12}\nu_{21})^2\}}{E_2(1 - \nu_{12}\nu_{21})}. \end{aligned} \tag{45}$$

Furthermore, substituting Eqs. (38) and (42) into Eq. (44), the following governing equation of the displacement field was obtained:

$$\frac{\partial^2 v}{\partial x^2} + \lambda^2 \frac{\partial^2 v}{\partial y^2} = 0, \tag{46}$$

where

$$\lambda = \sqrt{\frac{C_1 + aC_2}{G_{23}(C_1^2 - C_2^2)}} = \sqrt{\frac{E_2 - G_{23}(\nu_{23} + \nu_{12}\nu_{21})}{G_{23}(1 - \nu_{12}\nu_{21})}}. \tag{47}$$

The boundary condition of the governing equation is written as

$$\sigma_{xy}(0, y) = 0 \Leftrightarrow \frac{\partial v}{\partial x}(0, y) = 0, \tag{48}$$

$$v(t, y) = \varepsilon_{yy}^{\infty}, \tag{49}$$

$$v(x, 0) = 0, \tag{50}$$

$$\sigma_{yy}(x, l) = 0 \Leftrightarrow \frac{\partial v}{\partial y}(x, l) = 0, \tag{51}$$

where $\varepsilon_{yy}^{\infty}$ is the applied strain of the ply parallel to the y-axis and $2t$ is the ply thickness. The displacement field can be solved with Eq. (46). In our previous study,[29] this partial differential equation was solved by the variable separation method. However, the obtained solution was an infinite series and very complicated. Therefore, this study obtained a simplified form of the displacement field.

To obtain the simplified solution, the displacement form of the following type was assumed:

$$v(x, y) = A(y)x^2 + B(y)x + C(y). \tag{52}$$

Using the displacement in Eq. (52) in Eqs. (48) and (49) yielded

$$B(y) = 0, \tag{53}$$

$$C(y) = \varepsilon_{yy}^{\infty} y - A(y)t^2. \tag{54}$$

Thus, Eq. (52) can be written as

$$v(x, y) = A(y)(x^2 - t^2) + \varepsilon_{yy}^{\infty} y. \tag{55}$$

Next, our main task was to explicitly determine $A(y)$. The boundary condition of Eq. (50) gives

$$A(0) = 0. \tag{56}$$

However, it is impossible to satisfy the boundary condition of Eq. (51) exactly as it is. Thus, according to McCartney,[17] the following averaged boundary condition was used:

$$\frac{1}{t}\int_0^t \frac{\partial v(x,l)}{\partial y} dx = 0. \tag{57}$$

Hence, using Eq. (55) into Eq. (57) results in

$$\frac{dA(l)}{dy} = \frac{3\varepsilon_{yy}^{\infty}}{2t^2}. \tag{58}$$

Similar to Eq. (51), the government equation, i.e., Eq. (46), cannot be solved directly. Instead of Eq. (46), the following averaged government equation was here solved.

$$\frac{1}{t}\int_0^t \left(\frac{\partial^2 v}{\partial x^2} + \lambda^2 \frac{\partial^2 v}{\partial y^2}\right) dx = 0 \tag{59}$$

Using Eq. (55) in Eq. (59) yielded the following ordinary differential equation

$$\frac{d^2 A(y)}{dy^2} - \beta^2 A(y) = 0, \tag{60}$$

where

$$\beta = \frac{\sqrt{3}}{\lambda t}. \tag{61}$$

The solution of Eq. (60) with the boundary conditions in Eqs. (56) and (58) is

$$A(y) = \frac{3\varepsilon_{yy}^{\infty}}{2t^2\beta} \frac{\sinh \beta y}{\cosh \beta l}. \tag{62}$$

Thus, it can be shown that

$$v(x,y) = \frac{3\varepsilon_{yy}^{\infty}}{2t^2\beta} \frac{\sinh \beta y}{\cosh \beta l}(x^2 - t^2) + \varepsilon_{yy}^{\infty} y. \tag{63}$$

As stated in our previous paper,[29] the damage variable is the ratio of the inelastic strain due to crack opening to the total strain and is finally given by

$$d_{22} = \frac{\varepsilon_{yy}^{\infty} - \frac{1}{lt}\int_0^t v(x,l)dx}{\varepsilon_{yy}^{\infty}} = \frac{\tanh \beta l}{\beta l} = \frac{2\rho}{\beta} \tanh \frac{\beta}{2\rho}, \tag{64}$$

where $\rho = 1/(2l)$ is the transverse crack density in the damaged ply. As stated above, we derived the following equation:[29]

$$d_{22} = 1 - \frac{8}{\pi^3 \lambda t} \sum_{n=1}^{\infty} \frac{1}{(2n-1)^3} \frac{\tanh[(2n-1)\pi\lambda t\rho]}{\rho}. \tag{65}$$

Equation (64) is obviously simpler than Eq. (65) and loosening the boundary condition Eq. (51) increases crack opening, so that Eq. (64) gives better predictions than Eq. (65) in some cases. We will describe this section later through verifications and validations.

Damage variable d_{12} associated with transverse cracking When the effective compliance matrix shown in Eq. (18) is used, the analytical form for damage variable d_{12} is required. The schematic shown in Fig. 1 is also considered here. The neighboring ply deforms under a constant shear strain γ_{yz}^{∞} in the yz plane and the displacement field is assumed as

$$u(x, y, z) = v(x, y, z) = 0, \tag{66}$$

$$w = w(x, y). \tag{67}$$

Thus, these equations give $\sigma_x = \sigma_y = \sigma_z = \sigma_{xy} = 0$ and $\varepsilon_x = \varepsilon_y = \varepsilon_z = \gamma_{xy} = 0$, so that the out of plane shear stresses are nonzero and given as

$$\sigma_{xz}(x, y) = G_{12}\gamma_{xz}(x, y) = G_{12}\frac{\partial w(x, y)}{\partial x}, \tag{68}$$

$$\sigma_{yz}(x, y) = G_{12}\gamma_{yz}(x, y) = G_{12}\frac{\partial w(x, y)}{\partial y}. \tag{69}$$

The stresses should satisfy the following three-dimensional equilibrium equations:

$$\frac{\partial \sigma_{xx}}{\partial x} + \frac{\partial \sigma_{xy}}{\partial y} + \frac{\partial \sigma_{xz}}{\partial z} = 0, \tag{70}$$

$$\frac{\partial \sigma_{xy}}{\partial x} + \frac{\partial \sigma_{yy}}{\partial y} + \frac{\partial \sigma_{yz}}{\partial z} = 0, \tag{71}$$

$$\frac{\partial \sigma_{xz}}{\partial x} + \frac{\partial \sigma_{yz}}{\partial y} + \frac{\partial \sigma_{zz}}{\partial z} = 0. \tag{72}$$

These stresses given in Eqs. (68) and (69) automatically satisfy Eqs. (70) and (71) and leads to the following governing equation derived from Eq. (72):

$$\frac{\partial^2 w}{\partial x^2} + \frac{\partial^2 w}{\partial y^2} = 0. \tag{73}$$

As mentioned in the previous section, the following boundary conditions should be satisfied:

$$\sigma_{xz}(0,y)=0 \Leftrightarrow \frac{\partial w}{\partial x}(0,y)=0, \tag{74}$$

$$w(t,y)=\gamma_{yz}^{\infty} y, \tag{75}$$

$$w(x,0)=0, \tag{76}$$

$$\sigma_{yz}(x,l)=0 \Leftrightarrow \frac{\partial w}{\partial y}(x,l)=0. \tag{77}$$

This boundary problem defined by Eqs. (73)-(77) is almost the same as the one defined by Eqs. (46)-(51); therefore, the same derivation procedure can be adopted for this boundary problem. Thus, the displacement field is given by

$$w(x,y)=\frac{3\gamma_{yz}^{\infty}}{2t^2\beta_{12}}\frac{\sinh\beta_{12}y}{\cosh\beta_{12}l}(x^2-t^2)+\gamma_{yz}^{\infty}y, \tag{78}$$

$$\beta_{12}=\frac{\sqrt{3}}{t}. \tag{79}$$

The shear damage variable d_{12} can be defined as

$$d_{12}=1-\frac{G_{12}^{d}}{G_{12}}, \tag{80}$$

where G_{12}^{d} is the shear stiffness of the ply with transverse cracking. The average ply shear strain $\gamma_{yz}^{\mathrm{ave}}$ not considering the crack-opening displacement and applied shear strain γ_{yz}^{∞} are described as follows:

$$\gamma_{yz}^{\mathrm{ave}}=1-\frac{\sigma_{yz}}{G_{12}}, \tag{81}$$

$$\gamma_{yz}^{\infty}=1-\frac{\sigma_{yz}}{G_{12}^{d}}. \tag{82}$$

Substituting Eqs. (81) and (82) into Eq. (80), d_{12} can be rewritten as

$$d_{12}=1-\frac{\gamma_{yz}^{\mathrm{ave}}}{\gamma_{yz}^{\infty}}. \tag{83}$$

The average shear strain is defined by

$$\gamma_{yz}^{\mathrm{ave}}=\frac{1}{lt}\int_0^t w(x,l)dx. \tag{84}$$

We obtained d_{12} from Eqs. (78), (83), and (84).

$$d_{12}=\frac{\gamma_{yz}^{\infty}-\frac{1}{lt}\int_0^t w(x,l)dx}{\gamma_{yz}^{\infty}}=\frac{\tanh\beta_{12}l}{\beta_{12}l}=\frac{2\rho}{\beta_{12}}\tanh\frac{\beta_{12}}{2\rho} \tag{85}$$

The reduction in shear modulus was initially determined by Hashin,[11] by using the variation approach. Recently, Onodera and Okabe[32] also obtained the shear damage variable with an infinite series.

$$d_{12} = 1 - \frac{8}{\pi^3 t} \sum_{n=1}^{\infty} \frac{1}{(2n-1)^3} \frac{\tanh[(2n-1)\pi t\rho]}{\rho} \tag{86}$$

However, Eq. (85) is obviously simpler than the infinite series of Eq. (86).

Effective elastic constants for the damaged composite laminates

The substitution of damage variables d_{22} and d_{12} into Eqs. (1), (2), (8), and (18) gives the effective compliance/stiffness matrix of a ply with transverse cracks as a function of crack density ρ, and fiber breaks can be considered by substituting d_{11} into Eqs. (1), (2), and (18). The effective stiffness of composite laminates with transverse cracks can be estimated through the CLT using the effective compliance matrix of a damaged ply.

Let us consider the coordinate systems shown in Fig. 2. The effective compliance matrix and thermal expansion coefficient of the kth ply having transverse crack density ρ in material coordinate system $(1, 2, 3)$ are defined as $\boldsymbol{C}_k(\rho)$ and $\boldsymbol{\alpha}_k$, respectively. Similarly, those of laminate coordinate system (X, Y, Z) are defined as $\overline{\boldsymbol{C}}_k(\rho)$ and $\overline{\boldsymbol{\alpha}}_k$, respectively. When the fiber angle is given by θ_k, $\overline{\boldsymbol{C}}_k(\rho)$ and $\overline{\boldsymbol{\alpha}}_k$ are given as

$$\overline{\boldsymbol{C}}_k(\rho) = \boldsymbol{R}_k \boldsymbol{C}_k(\rho) \boldsymbol{T}_k^{-1}, \tag{87}$$

$$\overline{\boldsymbol{\alpha}}_k = \boldsymbol{R}\boldsymbol{\alpha}_k, \tag{88}$$

where

$$\boldsymbol{\alpha}_k = \begin{bmatrix} \alpha_{11} & \alpha_{22} & 0 \end{bmatrix}^{\mathrm{T}}, \tag{89}$$

$$\boldsymbol{R}_k = \begin{bmatrix} \cos^2\theta_k & \sin^2\theta_k & -\sin\theta_k\cos\theta_k \\ \sin^2\theta_k & \cos^2\theta_k & \sin\theta_k\cos\theta_k \\ 2\sin\theta_k\cos\theta_k & -2\sin\theta_k\cos\theta_k & \cos^2\theta_k - \sin^2\theta_k \end{bmatrix}, \tag{90}$$

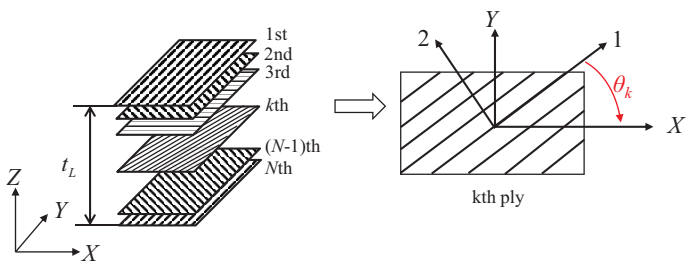

Figure 2. Relationship between the laminate coordinate system (X, Y, Z) and material coordinate system $(1, 2, 3)$.

$$\boldsymbol{T}_k = \begin{bmatrix} \cos^2\theta_k & \sin^2\theta_k & -2\sin\theta_k\cos\theta_k \\ \sin^2\theta_k & \cos^2\theta_k & 2\sin\theta_k\cos\theta_k \\ \sin\theta_k\cos\theta_k & -\sin\theta_k\cos\theta_k & \cos^2\theta_k - \sin^2\theta_k \end{bmatrix}. \tag{91}$$

α is the thermal expansion coefficient. Therefore, according to the CLT, the effective laminate strain $\overline{\varepsilon}_L$ is expressed as

$$\overline{\boldsymbol{\varepsilon}}_L = \overline{\boldsymbol{C}}_L \overline{\boldsymbol{\sigma}}_L + \overline{\boldsymbol{\alpha}}_L \Delta T, \tag{92}$$

where the effective stiffness matrix $\overline{\boldsymbol{C}}_L(\rho)$ and thermal expansion coefficient $\overline{\boldsymbol{\alpha}}_L(\rho)$ of the cracked laminate can be written as

$$\overline{\boldsymbol{C}}_L(\rho) = \left[\overline{C}_{Lij}\right] = \left[\frac{1}{t_L}\sum_{k=1}^{N} t_k \overline{\boldsymbol{C}}_k^{-1}(\rho)\right]^{-1}, \tag{93}$$

$$\overline{\boldsymbol{\alpha}}_L(\rho) = \left[\overline{\alpha}_{Li}\right] = \overline{\boldsymbol{C}}_L \left[\frac{1}{t_L}\sum_{k=1}^{N} t_k \overline{\boldsymbol{C}}_k^{-1}(\rho)\overline{\boldsymbol{\alpha}}_k\right]. \tag{94}$$

$\overline{\boldsymbol{\sigma}}_L$ is the applied axial laminate stress, t_L is the thickness of the corresponding composite laminates, and $\Delta T\,(= T - T_{\mathrm{sf}})$ is the difference between the testing temperature T and stress-free temperature T_{sf}. Therefore, the effective elastic constants and effective thermal expansion coefficients of the laminates are given as

$$E_X = \frac{1}{\overline{C}_{11}(\rho)}, \quad E_Y = \frac{1}{\overline{C}_{22}(\rho)}, \quad \nu_{XY} = -\frac{\overline{C}_{12}(\rho)}{\overline{C}_{11}(\rho)}, \quad G_{XY} = \frac{1}{\overline{C}_{66}(\rho)}, \tag{95}$$

$$\alpha_X = \overline{\alpha}_{L1}(\rho), \quad \alpha_Y = \overline{\alpha}_{L2}(\rho). \tag{96}$$

We can derive the effective elastic constants analytically with the crack density and fiber breaks through the CLT. The stress-strain relationship of damaged laminates can be obtained using Eq. (92).

Results and Discussions

Verification of damage models

The stiffness reduction in laminates with transverse cracking was studied using five approaches for verifying the effective compliance/stiffness matrices and proposed damage variables d_{22} and d_{12}. Murakami_simplified shows the Murakami model using d_{22} expressed in a simplified form in Eq. (64). Yoshimura_simplified is the Yoshimura model with d_{22} expressed in a simplified form, identical to Murakami_simplified. Li_simplified is the Li model including the damage parameter ω in Eqs. (16) and (64), and constant damage parameter ξ in Eqs. (17) and (47). Maimí_simplified gives the Maimí model with simplified forms of d_{22} in Eq. (64) and d_{12} in Eq. (85). Maimí_infinite_series describes the result of the Maimí model with infinite forms of d_{22} in Eq. (65) and d_{12} in Eq. (86). In Li_simplified, the upper limit of the transverse crack density resulting

from the assumption of a small damage postulated in Li's effective stiffness matrix was determined in the same manner as in our previous study.[33] Table 1 presents the upper limit of the transverse crack density in GFRP laminates used in Li_simplified.

For verification, comparisons to results obtained using FEA are presented for $[90/0]_s$ GFRP cross-ply laminates. The material properties listed in Table 2 were used. Transverse cracks are assumed to exist in the 90° plies and face the outer surface. Gudmundson and Zang[22] calculated the reduction in Poisson's ratio and Young's modulus due to the increase in the transverse crack density. When the matrix crack faces the surface, the crack length should be doubled to include the surficial effect and satisfy the boundary condition. Therefore, we obtain

$$d_{22} = \frac{4\rho}{\beta} \tanh \frac{\beta}{4\rho}, \tag{97}$$

$$d_{12} = \frac{4\rho}{\beta_{12}} \tanh \frac{\beta_{12}}{4\rho}, \tag{98}$$

$$d_{22} = 1 - \frac{4}{\pi^3 \lambda t} \sum_{n=1}^{\infty} \frac{1}{(2n-1)^3} \frac{\tanh[2(2n-1)\pi\lambda t\rho]}{\rho}, \tag{99}$$

$$d_{12} = 1 - \frac{4}{\pi^3 t} \sum_{n=1}^{\infty} \frac{1}{(2n-1)^3} \frac{\tanh[2(2n-1)\pi t\rho]}{\rho}. \tag{100}$$

The comparison results are shown in Figs. 3 and 5. As for Young's modulus, all approaches reproduce the tendency of the results observed in FEA. When comparing Maimí_simplified and Maimí_infinite_series, it is shown that the simple forms of Eqs. (64) and (85) yielded results closer to the FEA results than the infinite series forms of Eqs. (65) and (86). Thus, Eqs. (65) and (86) gave smaller crack openings than the FEA results and loosening the boundary condition may improve the tendency of the crack opening displacement to match with those obtained using FEA. Murakami_simplified, Li_simplified, Maimí_simplified and Maimí_infinite_series captured the degradation tendency of the Poisson's ratio; however, Yoshimura_simplified

Table 1. Upper limit of transverse crack density used in Li_simplified.

Laminte	Upper limit of transverse crack density (cracks/mm)
GFRP $[90/0]_s$	2.01
GFRP $[55/-55]_N$	4.02

Table 2. Material constants and thickness of GFRP ply used in stiffness reduction calculation.[22]

E_1 (GPa)	E_2 (GPa)	ν_{12}	ν_{23}	G_{12} (GPa)	G_{23} (GPa)	α_1 (/℃)	α_2 (/℃)	Ply thickness (mm)
41.7	13	0.3	0.42	3.4	4.58	6.72 $\times 10^{-6}$	29.3 $\times 10^{-6}$	0.203

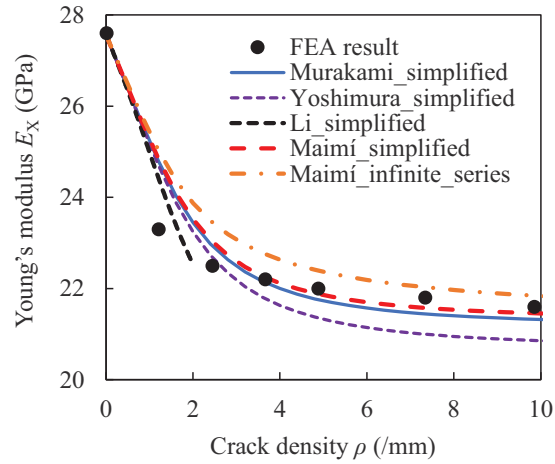

Figure 3. Comparison of Young's modulus reduction in GFRP $[90/0]_s$ laminate due to transverse crack predicted using present models and FEA (Gudmundson and Zhang[22]).

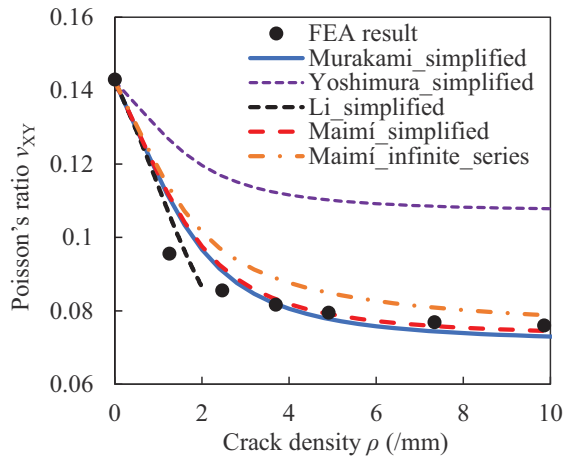

Figure 4. Comparison of Poisson's ratio reduction in GFRP $[90/0]_s$ due to transverse cracking predicted using present models and FEA (Gudmundson and Zhang[22]).

obviously underestimated the degradation. This causes the significant errors in the case of angle-ply laminates because the non-diagonal component directly affects the Young's modulus of the laminate.

Gudmundson and Zhang[22] also calculated the stiffness reduction in several types of angle-ply laminates using FEA. The present model was verified by comparison with the results for $[\pm 55]_N$ angle-ply GFRP laminates. The material properties listed in Table

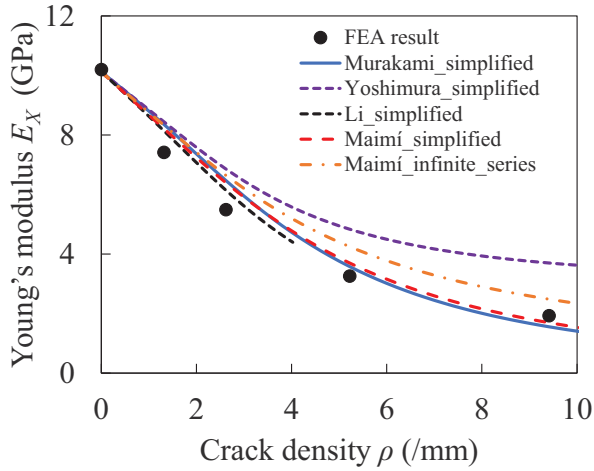

Figure 5. Comparison of Young's moduli of GFRP $[\pm 55]_N$ axial laminates due to transverse cracking predicted by present models and FEA (Gudmundson and Zhang[22]).

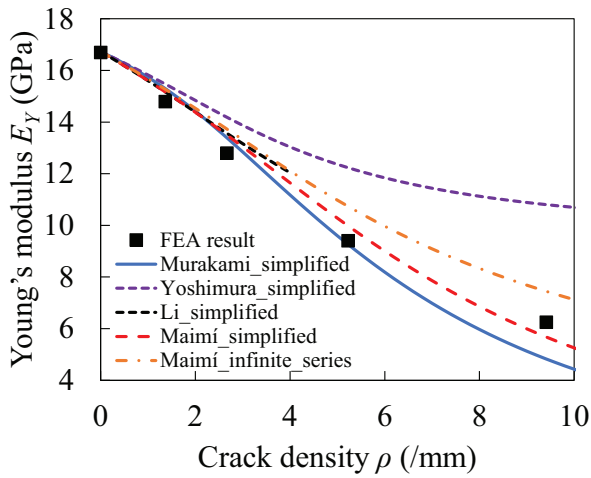

Figure 6. Comparison of Young's moduli reduction in GFRP $[\pm 55]_N$ transverse laminate due to transverse cracking predicted by present models and FEA (Gudmundson and Zhang[22]).

2 were used. Figures 5 - 10 show the changes in the Young's moduli, shear modulus, Poisson's ratio, and thermal expansion coefficients of $[\pm 55]_N$ laminate as a function of the transverse crack density. Clearly, Maimí_simplified shows the best agreement among these five approaches for any of the elastic constants, whereas Yoshimura_simplified cannot capture the trends of Young's modulus and Poisson's ratio at all. As stated above,

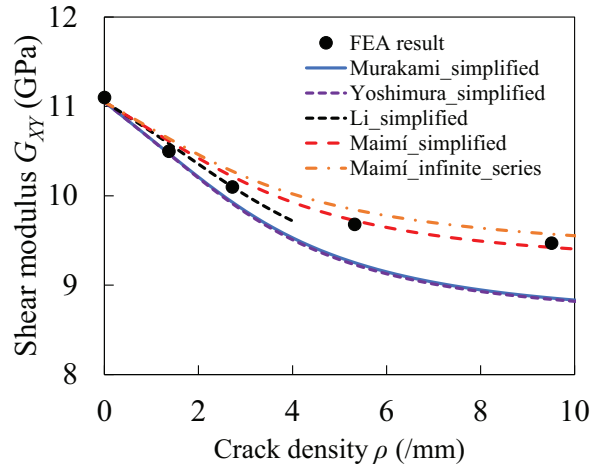

Figure 7. Comparison of shear modulus reduction in GFRP $[\pm 55]_N$ laminate due to transverse cracking predicted by present models and FEA (Gudmundson and Zhang[22]).

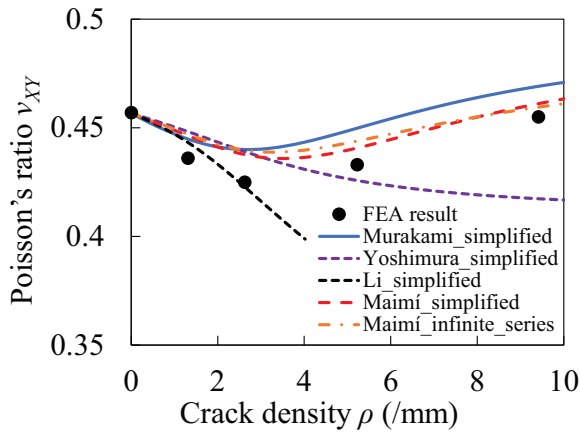

Figure 8. Comparison of Poisson's ratio change in GFRP $[\pm 55]_N$ laminate due to transverse cracking predicted by present models and FEA (Gudmundson and Zhang[22]).

Poisson's ratio is a critical parameter for evaluating the properties of angle-ply laminates as it reflects the behavior of non-diagonal components in compliance/stiffness matrix. The trends of Yoshimura_simplified are substantially different from those observed in FEA. Therefore, we do not recommend using Yoshimura_simplified for evaluating angle-ply laminates.

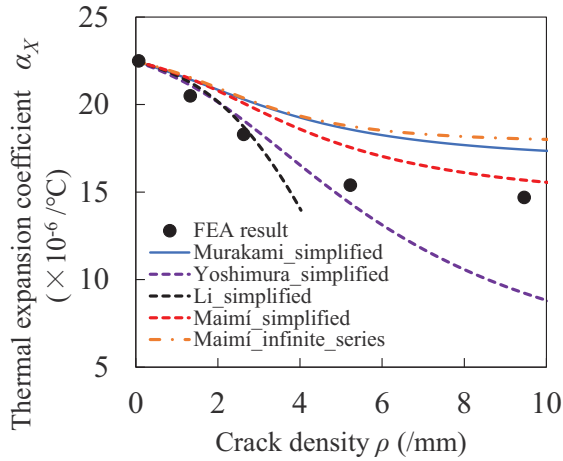

Figure 9. Comparison of axial laminate thermal expansion coefficient reduction in GFRP $[\pm 55]_N$ due to transverse cracking predicted by present models and FEA (Gudmundson and Zhang[22]).

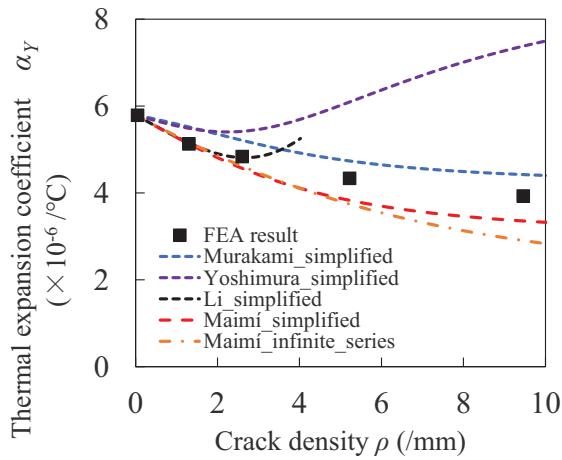

Figure 10. Comparison of transverse laminate thermal expansion coefficient reduction in GFRP $[\pm 55]_N$ due to transverse cracking predicted by present models and FEA (Gudmundson and Zhang[22]).

Although the results obtained using all the models agree well with the FEA results, Maimí_simplified shows the best agreement. In fact, we proved that Maimí_simplified is the most appropriate approach among five approaches considering in this study.

Nonlinear stress-strain response of CFRP cross-ply laminates

The nonlinear stress-strain response of CFRP cross-ply laminates resulting from transverse cracking was calculated using the present model and compared to the experimental results obtained in this study. We also applied our model to the results reported by Fikry et al.[42] The stress-strain response of cross-ply laminates with transverse cracking was calculated using Eqs. (92)-(94). From the verification result described in the previous section, the effective stiffness model of Maimí_simplified composed of the Maimí model with simplified forms of d_{22} in Eq. (64) and d_{12} in Eq. (85) was utilized to predict the stiffness reduction due to transverse cracks in 90° plies. In CFRP laminates subjected to quasi-static monotonic tensile loading, fiber fracture often occurs at the ultimate failure stress of the laminate. Therefore, the stiffness reduction owing to fiber breaks was not considered here, and the ultimate tensile strength of CFRP cross-ply laminates was predicted based on a strain-based fiber failure criterion presented by McCartney[27] to determine the fracture point in the nonlinear stress-strain curve. In this criterion, the calculated effective laminate axial strain using Eq. (92) is considered equal to the fiber axial strain in 0° plies. When the effective laminate axial strain is equal to the critical strain, ε_{fc}, during ultimate fiber failure, ultimate failure of the laminate occurs. The ultimate fiber failure strain, ε_{fc}, is derived from the spring element model (SEM) simulation,[43] which considers the surficial stress concentration obtained from multiple-fiber fragmentation tests.[44] The bimodal Weibull distribution was applied to reproduce the statistically distributed strength in fibers. A stress concentration factor of 1.9 was used. The average ultimate fiber failure strain obtained by 100 SEM simulations scaled with each specimen size, was regarded as the ultimate fiber failure strain ε_{fc}. Table 3 lists the material properties of the T700S and resin and Table 4 shows bimodal Weibull parameters of the T700S fiber used in SEM simulations. The evolution of transverse crack density ρ as a function of the applied laminate stress is needed to predict the nonlinear stress-strain curves of the laminates. In this study, to validate the proposed stiffness reduction model, we assumed the following Weibull form for transverse crack density evolution:

$$\rho = \rho_s \left[1 - \exp\left\{ - \left(\frac{\overline{\sigma}_L - \sigma_{L0}}{\sigma_{Lc}} \right)^{m_T} \right\} \right], \tag{101}$$

Table 3. Properties of T700S fiber and resin used in SEM simulations.[45]

Fiber axial Young's modulus E_f (GPa)	230
Fiber radius r (μm)	3.5
Matrix Young's modulus E_m (GPa)	3.4
Matrix Poisson's ratio ν_m (-)	0.31

Table 4. Bimodal Weibull parameters of the T700S fiber used in SEM simulations.[44]

σ_{01} (GPa)	m_1	σ_{02} (GPa)	m_2
5.2	4.8	6.1	12.0

where ρ_s is the saturated transverse crack density, σ_{L0} is the initiation stress of the transverse crack, σ_{Lc} is the Weibull scale parameter, and m_T is the Weibull modulus. These parameters were determined by fitting with the experimental results.

We performed the experiments by ourselves to validate our model presented in this study. Here, we briefly explain the experimental procedures followed to determine the stiffness reduction, transverse crack density, and stress-strain curves of the cross-ply laminates. Loading and unloading tests were conducted to obtain the nonlinear stress-strain response of cross-ply laminates, transverse crack density in 90° plies, and stiffness reduction. The $[0/90_8/0]$ cross-ply laminate was composed of T700S/2592 (Toray Industries) unidirectional plies. The laminate specimen had a length, width, and thickness of 249, 25, and 1.42 mm, respectively. A strain gauge (Kyowa Electronic Instruments Co.) was used to measure the strain in the laminate. The free edge of the laminate was polished by a diamond grinding disk (Buehler Ltd.) to observe the transverse crack density. Loading and unloading tests were performed using a servo-hydraulic testing machine MTS810 (MTS Systems Corporation) and involved the following steps. (1) The specimen was loaded with a crosshead speed 1.0 mm/min. (2) When the load reached a specific value, the specimen was held at this load and the transverse cracks were observed at the free edge of the specimen using RepliSet (Struers). (3) The specimen was then unloaded with a crosshead speed 1.0 mm/min until the load reached zero. This loading/unloading cycle comprising steps (1)-(3) was repeated until the specimen failed.

The stress-strain relationship for the T700S/2592 $[0/90_8/0]$ laminate predicted from the present model was compared to the obtained experiment results. We denote T700S/2592 as CFRP-I. The material properties of the ply, parameters of transverse crack evolution, and ultimate fiber failure strain, ε_{fc}, derived from SEM simulations are listed in Tables 5, 6, and 7, respectively. The out-of-plane shear modulus, G_{23}, of CFRP-I ply given in Table 5 was derived as follows:

$$G_{23} = \frac{E_2}{2(1+\nu_{23})}. \tag{102}$$

Parameters of transverse crack density evolution were determined by fitting the calculated results of the present model with the experimental data as shown in Fig. 11 (a). Figure 11 (b) presents a comparison of the predicted results for stiffness reduction as a function of transverse crack density determined by using the present model with experimental results. The results predicted using the present model agree quantitatively with the experimental results obtained through loading/unloading tests. The predicted stress-strain responses of the T700S/2592 $[0/90_8/0]$ laminate was compared to the experimental results, as shown in Fig. 11 (c). The results of the present model obtained considering stiffness reduction due to transverse cracking show good agreement with the experimental data. According to these results, the nonlinearity of the stress-strain responses observed in the 200-350 MPa range is mainly due to transverse cracking. The ultimate failure stress and strain determined from the critical-strain-based criterion also agree with the experimental data. This result implies that the ultimate failure strength of CFRP laminates with 0° plies can be determined using the strain-based fiber criterion,

Table 5. Mechanical properties of plies used in the calculation of stress-strain behavior of cross-ply laminates.

	CFRP-I[46]	CFRP-II[42]
Longitudinal Young's modulus E_1 (GPa)	115	123
Transverse Young's modulus E_2 (GPa)	7.74	8.68
In-plane Poisson's ratio ν_{12} (-)	0.315	0.33
Out-of-plane Poisson's ratio ν_{23} (-)	0.394	0.394[c]
In-plane shear modulus G_{12} (GPa)	3.54	3.92
Out-of-plane shear modulus G_{23} (GPa)	3.78[a]	2.91[a]
Longitudinal thermal expansion coefficient α_1 (10^{-6}/℃)	0.4[b]	0.4[b]
Transverse thermal expansion coefficient α_2 (10^{-6}/℃)	36[b]	36[b]
Temperature difference ΔT (℃)	-100	-110
Fiber volume fraction f (-)	0.51	0.528[d]
Ply thickness (mm)	0.142	0.15

[a] G_{23} was estimated using Eq. (102).
[b] These values are quoted from Okabe et al.[45]
[c] This value is quoted from Kumagai et al.[46]
[d] This was estimated from Eq. (103). E_f and E_m given in Table 3 were used.

Table 6. Simulation results of ultimate fiber failure strain at stress concentration factor of 1.9.

	CFRP-I	CFRP-II
Ultimate fiber failure strain ε_{fc} (%)	1.77	1.83

Table 7. Parameters of transverse crack evolution in CFRP laminate used in Eq. (102).

	CFRP-I	CFRP-II
σ_{L0} (MPa)	180	180
σ_{Lc} (MPa)	74	110
m_T	1.5	1.7
ρ_s (/mm)	0.76	0.9

and the ultimate fiber failure strain used in this criterion can be predicted through SEM simulations.

The nonlinear stress-strain behavior of the T700SC/2592 $[0/90_8/0]$ laminate was predicted using the present model and the results were compared to the experimental result obtained by Fikry et al.[42] We denote T700SC/2592 as CFRP-II. The material properties of the ply, parameters of transverse crack evolution, and ultimate fiber failure strain, ε_{fc}, derived from SEM simulations are also listed in Table 5, 6, and 7, respectively. The out-of-plane shear modulus G_{23} of CFRP-II ply given in Table 5 was estimated using Eq. (102). The fiber volume fraction, f, of CFRP-II is estimated as

$$f = \frac{E_1 - E_m}{E_f - E_m}, \tag{103}$$

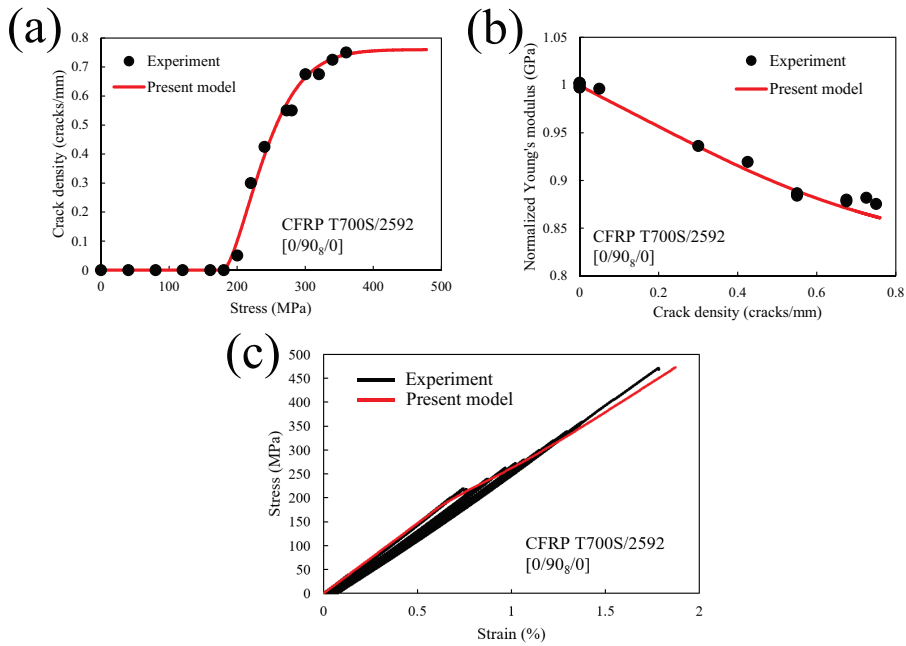

Figure 11. Comparison of results predicted using present model for (a) transverse crack density evolution, (b) stiffness reduction, and (c) stress-strain response of T700S/2592 $[0/90_8/0]$ laminate with experimental results.

where E_f is the fiber axial Young's modulus and E_m is the matrix Young's modulus given in Table 3. The crack evolution parameters used in Eq. (101) were derived by fitting the predicted results with the experiment results, as shown in Fig. 12 (a). The predicted results for stiffness reduction as a function of the transverse crack density show excellent agreement with the experimental results, as shown in Fig. 12 (b). Figure 12 (c) presents the nonlinear stress as a function of the longitudinal or transverse strain obtained using the present model and through experiments. The present model considering the stiffness reduction due to transverse cracks can predict the nonlinearity of the stress-strain response up to the ultimate failure strength of the laminate estimated using the critical-strain-based criterion.

Nonlinear stress-strain response of GFRP cross-ply laminates

The nonlinear stress-strain behavior of E-glass/TX24235 GFRP $[0/90_n/0]_s$ $(n = 2, 4, 6)$ laminates was predicted to validate our proposed damage variables d_{11}, d_{22}, and d_{12}. The stress-strain responses of cross-ply laminates with transverse cracking and fiber breaks were calculated using Eqs. (92)-(94). The effective stiffness model Maimí_simplified comprising of the Maimí model with simplified forms of d_{22} in Eq. (64) and d_{12} in Eq. (85) was utilized to predict the stiffness reduction due to transverse cracks in 90° plies. In

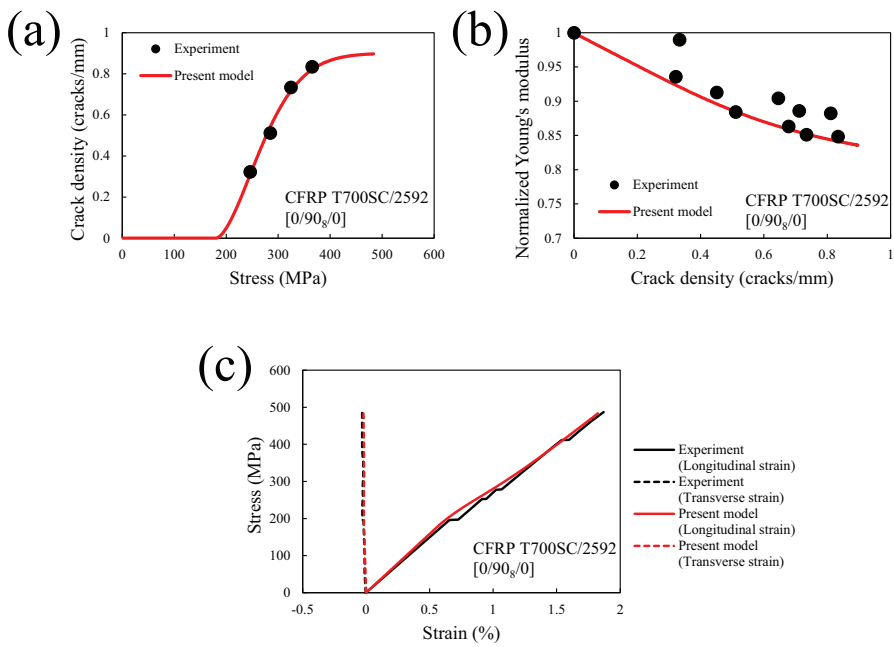

Figure 12. Comparison of (a) transverse crack density, (b) stiffness reduction, and (c) stress-strain response of T700SC/2592 $[0/90_8/0]$ predicted using the present model with experimental results (Fikry et al.[42]).

the case of GFRP laminates, the stiffness reduction due to multiple-fiber fragmentation in 0° plies and subsequent final laminate failure was calculated using damage variable d_{11} in Eq. (28).

The GFRP ply properties were estimated using the analytical model developed by Kravchenko et al.[47] According to them, the properties of unidirectional-fiber-reinforced ply composed of the transversely isotropic fibers and the isotropic matrix are determined as follows:

$$E_1 = E_1^{(f)} f^{(f)} + E^{(m)} f^{(m)} + \left[\frac{4(\nu^{(m)} - \nu_{12}^{(f)})^2 k^{(m)} k^{(f)} G^{(m)}}{(k^{(f)} + G^{(m)}) k^{(m)} + (k^{(f)} - k^{(m)}) G^{(m)} f^{(f)}} \right] f^{(f)} f^{(m)}, \tag{104}$$

$$E_2 = \left[\frac{1}{4k_2} + \frac{1}{4G_{23}} + \frac{\nu_{12}^2}{E_1} \right]^{-1}, \tag{105}$$

$$\nu_{12} = \nu_{12}^{(f)} f^{(f)} + \nu^{(m)} f^{(m)} + \left[\frac{(\nu^{(m)} - \nu_{12}^{(f)})(k^{(m)} - k^{(f)}) G^{(m)}}{(k^{(f)} + G^{(m)}) k^{(m)} + (k^{(f)} - f^{(m)}) G^{(m)} f^{(f)}} \right] f^{(f)} f^{(m)}, \tag{106}$$

$$\nu_{23} = 1 - \frac{E_2}{2k_2} - 2\nu_{12}^2 \frac{E_2}{E_1}, \tag{107}$$

$$G_{12} = G^{(m)} \left[\frac{(G_{12}^{(f)} + G^{(m)}) + (G_{12}^{(f)} - G^{(m)}) f^{(f)}}{(G_{12}^{(f)} + G^{(m)}) - (G_{12}^{(f)} - G^{(m)}) f^{(f)}} \right], \tag{108}$$

$$G_{23} = G^{(m)} \left[\frac{(G_{23}^{(f)} + G^{(m)}) k^{(m)} + 2G_{23}^{(f)} G^{(m)} + (G_{23}^{(f)} - G^{(m)}) k^{(m)} f^{(f)}}{(G_{23}^{(f)} + G^{(m)}) k^{(m)} + 2G_{23}^{(f)} G^{(m)} - (G_{23}^{(f)} - G^{(m)})(k^{(m)} + 2G^{(m)}) f^{(f)}} \right], \tag{109}$$

$$\alpha_1 = \frac{\alpha_1^{(f)} E_1^{(f)} + \alpha^{(m)} E^{(m)} f^{(m)}}{E_1^{(f)} f^{(f)} + E^{(m)} f^{(m)}}, \tag{110}$$

$$\alpha_2 = (\alpha_2^{(f)} + \nu_{12}^{(f)} \alpha_1^{(f)}) f^{(f)} + (1 + \nu^{(m)}) \alpha^{(m)} f^{(m)} - (\nu_{12}^{(f)} f^{(f)} + \nu^{(m)} f^{(m)}) \alpha_1, \tag{111}$$

where

$$k^{(f)} = \frac{E_1^{(f)} E_2^{(f)}}{2(1 - \nu_{23}^{(f)}) E_1^{(f)} - 4 \left(\nu_{12}^{(f)}\right)^2 E_2^{(f)}}, \tag{112}$$

$$k^{(m)} = \frac{E^{(m)}}{2(1 - \nu^{(m)}) - 4 \left(\nu^{(m)}\right)^2}, \tag{113}$$

$$k_2 = \frac{(k^{(f)} + G^{(m)}) k^{(m)} + (k^{(f)} - k^{(m)}) G^{(m)} f^{(f)}}{(k^{(f)} + G^{(m)}) - (k^{(f)} - k^{(m)}) f^{(f)}}. \tag{114}$$

Here, superscripts (f) and (m) denote the fiber and matrix property, respectively. Subscripts 1, 2, and 3 represent the material coordinate axis of the ply shown in Fig. 1. E, G, ν, α, k, and f are the Young's modulus, shear modulus, Poisson's ratio, thermal expansion coefficient, bulk modulus, and volume fraction, respectively. k_2 is the transverse plane bulk modulus. $E_1^{(f)} = E_2^{(f)} = E^{(f)}$, $G_{12}^{(f)} = G_{23}^{(f)} = G^{(f)}$, $\nu_{12}^{(f)} = \nu_{23}^{(f)} = \nu^{(f)}$, and $\alpha_1^{(f)} = \alpha_2^{(f)} = \alpha^{(f)}$ are assumed because the E-glass fiber is isotropic. Table 8 lists the material properties of the E-glass fiber and resin used in Eqs. (104)-(114). Tables 9 and 10 present the material properties used for calculating d_{11} and the parameters of transverse crack evolution in Eq. (101), respectively. The crack evolution parameters were derived by fitting the results predicted by present model with the experimental results, as shown in Fig. 13 (a).

Figure 13 (b) shows the comparison of the stress-strain responses of E-glass/TX24235 GFRP $[0/90_n/0]_s$ $(n = 2, 4, 6)$ laminates with those obtained experimentally by Okabe et al.[50] The results predicted by the present model for the $[0/90_2/0]_s$ laminate does not agree with the experiment results. The present model overestimated the laminate failure strength, despite considering the stiffness reduction due to transverse cracking and fiber breaks. The reason for this overestimation may be the stiffness reduction, due to additional damage modes such as delamination resulting from stress concentration at the transverse crack tip. The predicted results for $[0/90_4/0]_s$ and $[0/90_6/0]_s$ laminates

Table 8. Material properties of E-glass fiber and resin.[48]

Fiber Young's Modulus $E^{(f)}$ (GPa)	72.4
Fiber Poisson's ratio $\nu^{(f)}$	0.2
Fiber shear modulus $G^{(f)}$ (GPa)	30.17
Fiber thermal expansion coefficient $\alpha^{(f)}$ $(10^{-5}/℃)$	0.5
Fiber volume fraction f	0.5
Matrix Young's modulus $E^{(m)}$ (GPa)	3.4
Matrix Poisson's ratio $\nu^{(m)}$	0.35
Matrix shear modulus $G^{(m)}$ (GPa)	1.259
Matrix thermal expansion coefficient $\alpha^{(m)}$ $(10^{-5}/℃)$	11.0

Table 9. Material properties used for calculating d_{11}.[49]

Fiber radius r (μm)	6.5
Gauge length L_0 (mm)	24
Weibull modulus m	6.34
Fiber strength σ_0 based on L_0 (MPa)	1550
Fiber/matrix interfacial shear stress τ (MPa)	25

Table 10. Parameters of transverse crack evolution in E-glass/TX24235 GFRP $[0/90_n/0]_s$ $(n = 2, 4, 6)$ laminates.

	$[0/90_2/0]_s$	$[0/90_4/0]_s$	$[0/90_6/0]_s$
σ_{L0} (MPa)	140	70	55
σ_{Lc} (MPa)	100	100	100
m_T	3.1	3.1	3.1
ρ_s (/mm)	21.5	16.0	10.5

reasonably agrees with the experimental results. Furthermore, the laminate failure strength derived from the GLS model can be used to predict the results. From the results described in the previous and current sections, we concluded that the present model can reproduce the stress-strain responses of cross-ply laminates with transverse cracks and fiber breaks using the Maimí model with damage variables d_{11}, d_{22}, and d_{12} proposed in this study.

Conclusions

This study involved deriving a new analytical model for predicting the effective compliance of composite laminates and simplified expressions for the damage tensor. We evaluated four models that yielded asymmetric/symmetric compliance matrices of damaged composite plies. Damage variable d_{11} describing stiffness reduction due to fiber breaks and its upper bound $d_{11}^{\max}$ given by $1/(m+2)$ were formulated using the GLS model. Moreover, the simplified analytical forms of damage variables d_{22} and d_{12} were developed, assuming that the displacement field along the longitudinal direction could be expressed as a quadric function by loosening the boundary condition for the governing

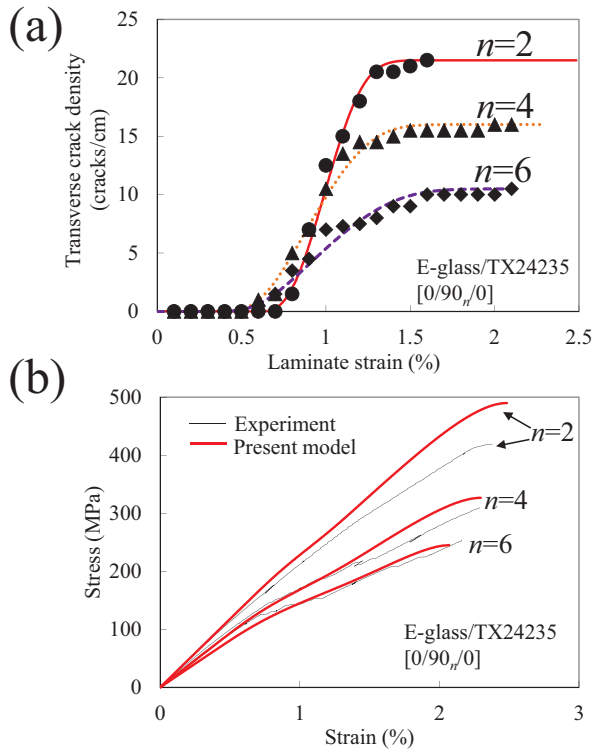

Figure 13. Comparison of (a) transverse cracking progression and (b) stress-strain responses of E-glass/TX24235 GFRP $[0/90_n/0]_s$ $(n = 2, 4, 6)$ laminates predicted using the present model with experimental results (Okabe et al.[50]).

differential equation. We also proved that the effective laminate properties could be obtained by substituting the damage variables into the CLT- and CDM-based models. Comparisons of the effective stiffness of laminates with transverse cracking to the results obtained via finite element calculations were performed for model verification. We found that the Maimí model[41] in combination with the proposed formulation for the damage variables, referred to as Maimí_simplified in this study, was the most appropriate model for predicting or estimating damage in composite laminates with transverse cracking.

The nonlinear stress-strain behaviors of CFRP cross-ply laminates resulting from transverse cracking were predicted using the present model, and the predicted results are compared with the experimental results. The effective compliance model with simplified damage variable d_{22} and d_{12} was utilized to calculate the stiffness reduction of the CFRP laminates. The ultimate tensile strength of CFRP cross-ply laminates was predicted based on a strain-based fiber failure criterion because fiber fracture in CFRP laminate occurs at the ultimate laminate failure stress. We assumed that the laminate failed when the effective axial laminate strain became equal to the ultimate fiber axial failure strain

in 0° plies. The ultimate fiber axial failure strain was derived from SEM simulations. The present model quantitatively reproduced the experimental results up to the ultimate failure strength of the laminate.

We predicted the nonlinear stress-strain behavior of $[0/90_n/0]_s$ $(n = 2, 4, 6)$ GFRP cross-ply laminates with transverse cracks in 90° plies and fiber breaks in 0° plies to validate our proposed damage tensor d_{11}, d_{22}, and d_{12}. d_{11} associated with fiber breaks and its upper bound describing the ultimate failure condition were analytically derived using the GLS model.[35] The effective stiffness model with simple damage variables d_{11}, d_{22}, and d_{12} was utilized to evaluate the stiffness reduction due to transverse cracking, fiber breaks, and ultimate failure of the laminate. In $[0/90_4/0]_s$ and $[0/90_6/0]_s$ laminates, the results predicted using the developed model showed reasonable agreement with the experimental results when the transverse cracking progression was fitted with the experimental results. Thus, if transverse cracking progression is formulated properly, the stress-strain diagram can be reproduced better.

Acknowledgements

This work was supported by Council for Science, Technology and Innovation (CSTI), Cross-ministerial Strategic Innovation Promotion Program (SIP), "Materials Integration" for revolutionary design system of structural materials (Funding agency: JST). The authors would like to acknowledge the vitally important encouragement and support made through the University of Washington-Tohoku University: Academic Open Space (UW-TU: AOS). This work was partly supported by Toray Industries, Inc. S. O. appreciates the support of JSPS KAKENHI Grant No. JP 18J20899. We would like to thank S. Date (Tohoku University) for his support in conducting the SEM simulations. We would also like to express our appreciation to S. Kochii (Tohoku University) for his assistance while performing experiments. The authors would like to thank Editage (www.editage.com) for English language editing.

Declaration of conflicting interests

The authors declare that there is no conflict of interest.

References

1. Parvizi A, Garrett KW and Bailey JE. Constrained cracking in glass fibre-reinforced epoxy cross-ply laminates. *Journal of Materials Science* 1978; 13(1): 195–201. DOI: 10.1007/BF00739291.
2. Parvizi A and Bailey JE. On multiple transverse cracking in glass fibre epoxy cross-ply laminates. *Journal of Materials Science* 1978; 13(10): 2131–2136. DOI:10.1007/BF00541666.
3. Garrett KW and Bailey JE. Multiple transverse fracture in 90° cross-ply laminates of a glass fibre-reinforced polyester. *Journal of Materials Science* 1977; 12(1): 157–168. DOI: 10.1007/BF00738481.
4. Garrett KW and Bailey JE. The effect of resin failure strain on the tensile properties of glass fibre-reinforced polyester cross-ply laminates. *Journal of Materials Science* 1977; 12(11): 2189–2194. DOI:10.1007/BF00552239.

5. Bailey JE and Parvizi A. On fibre debonding effects and the mechanism of transverse-ply failure in cross-ply laminates of glass fibre/thermoset composites. *Journal of Materials Science* 1981; 16(3): 649–659. DOI:10.1007/BF02402782.
6. Manders PW, Chou TW, Jones FR et al. Statistical analysis of multiple fracture in 0°/90°/0° glass fibre/epoxy resin laminates. *Journal of Materials Science* 1983; 18(10): 2876–2889. DOI:10.1007/BF00700768.
7. Cox HL. The elasticity and strength of paper and other fibrous materials. *British Journal of Applied Physics* 1952; 3(3): 72–79. DOI:10.1088/0508-3443/3/3/302.
8. Han Y, Hahn H and Croman R. A simplified analysis of transverse ply cracking in cross-ply laminates. *Composites Science and Technology* 1988; 31(3): 165–177. DOI:10.1016/0266-3538(88)90008-5.
9. Lee JW and Daniel I. Progressive Transverse Cracking of Crossply Composite Laminates. *Journal of Composite Materials* 1990; 24(11): 1225–1243. DOI:10.1177/002199839002401108.
10. Wang A, Chou P and Lei S. A Stochastic Model for the Growth of Matrix Cracks in Composite Laminates. *Journal of Composite Materials* 1984; 18(3): 239–254. DOI:10.1177/002199838401800304.
11. Hashin Z. Analysis of stiffness reduction of cracked cross-ply laminates. *Engineering Fracture Mechanics* 1986; 25(5-6): 771–778. DOI:10.1016/0013-7944(86)90040-8.
12. Hashin Z. Analysis of Orthogonally Cracked Laminates Under Tension. *Journal of Applied Mechanics* 1987; 54(4): 872–879. DOI:10.1115/1.3173131.
13. Lee JW, Allen D and Harris C. Internal State Variable Approach for Predicting Stiffness Reductions in Fibrous Laminated Composites with Matrix Cracks. *Journal of Composite Materials* 1989; 23(12): 1273–1291. DOI:10.1177/002199838902301205.
14. Talreja R. A Continuum Mechanics Characterization of Damage in Composite Materials. *Proceedings of the Royal Society A: Mathematical, Physical and Engineering Sciences* 1985; 399(1817): 195–216. DOI:10.1098/rspa.1985.0055.
15. Allen D, Harris C and Groves S. A thermomechanical constitutive theory for elastic composites with distributed damage-I. Theoretical development. *International Journal of Solids and Structures* 1987; 23(9): 1301–1318. DOI:10.1016/0020-7683(87)90107-7.
16. Allen D, Harris C and Groves S. A thermomechanical constitutive theory for elastic composites with distributed damage-II. Application to matrix cracking in laminated composites. *International Journal of Solids and Structures* 1987; 23(9): 1319–1338. DOI:10.1016/0020-7683(87)90108-9.
17. McCartney LN. Theory of stress transfer in a 0°-90°-0° cross-ply laminate containing a parallel array of transverse cracks. *Journal of the Mechanics and Physics of Solids* 1992; 40(1): 27–68. DOI:10.1016/0022-5096(92)90226-R.
18. Pagano N, Schoeppner G, Kim R et al. Steady-state cracking and edge effects in thermomechanical transverse cracking of cross-ply laminates. *Composites Science and Technology* 1998; 58(11): 1811–1825. DOI:10.1016/S0266-3538(98)00047-5.
19. Nairn JA and Hu S. The initiation and growth of delaminations induced by matrix microcracks in laminated composites. *International Journal of Fracture* 1992; 57(1): 1–24. DOI:10.1007/BF00013005.

20. Noda J, Okabe T, Takeda N et al. Damage Process of GFRP Cross-ply Laminates. *Transactions of the Japan Society of Mechanical Engineers Series A* 2004; 70(698): 1364–1369. DOI: 10.1299/kikaia.70.1364.
21. Xia Z, Carr R and Hutchinson J. Transverse cracking in fiber-reinforced brittle matrix, cross-ply laminates. *Acta Metallurgica Et Materialia* 1993; 41(8): 2365–2376. DOI: 10.1016/0956-7151(93)90316-K.
22. Gudmundson P and Zang W. An analytic model for thermoelastic properties of composite laminates containing transverse matrix cracks. *International Journal of Solids and Structures* 1993; 30(23): 3211–3231. DOI:10.1016/0020-7683(93)90110-S.
23. Dvorak GJ, Laws N and Hejazi M. Analysis of Progressive Matrix Cracking in Composite Laminates I. Thermoelastic Properties of a Ply with Cracks. *Journal of Composite Materials* 1985; 19(3): 216–234. DOI:10.1177/002199838501900302.
24. Dvorak GJ and Laws N. Analysis of Progressive Matrix Cracking In Composite Laminates II. First Ply Failure. *Journal of Composite Materials* 1987; 21(4): 309–329. DOI:10.1177/002199838702100402.
25. Kobayashi S, Ogihara S and Takeda N. Damage mechanics analysis for predicting mechanical behavior of general composite laminates containing transverse cracks. *Advanced Composite Materials* 2000; 9(4): 363–375. DOI:10.1163/15685510052000165.
26. Hajikazemi M and McCartney LN. Comparison of Variational and Generalized Plane Strain approaches for matrix cracking in general symmetric laminates. *International Journal of Damage Mechanics* 2018; 27(4): 507–540. DOI:10.1177/1056789516685381.
27. McCartney L. Energy-based prediction of progressive ply cracking and strength of general symmetric laminates using an homogenisation method. *Composites Part A: Applied Science and Manufacturing* 2005; 36(2): 119–128. DOI:10.1016/j.compositesa.2004.06.003.
28. Vinogradov V and Hashin Z. Variational analysis of cracked angle-ply laminates. *Composites Science and Technology* 2010; 70(4): 638–646. DOI:10.1016/j.compscitech.2009.12.018.
29. Okabe T, Onodera S, Kumagai Y et al. Continuum damage mechanics modeling of composite laminates including transverse cracks. *International Journal of Damage Mechanics* 2018; 27(6). DOI:10.1177/1056789517711238.
30. Murakami S. *Continuum Damage Mechanics*, *Solid Mechanics and Its Applications*, volume 185. Dordrecht: Springer Netherlands, 2012. ISBN 978-94-007-2665-9. DOI:10.1007/978-94-007-2666-6.
31. Kanagawa Y, Murakami S, Liu Y et al. Description of Internal Damage in FRP Laminates by Continuum Damage Mechanics. *Journal of the Society of Materials Science, Japan* 1996; 45(2): 206–211. DOI:10.2472/jsms.45.206.
32. Onodera S and Okabe T. Three-dimensional analytical model for effective elastic constants of transversely isotropic plates with multiple cracks: Application to stiffness reduction and steady-state cracking of composite laminates. *Engineering Fracture Mechanics* 2019; 219(April): 106595. DOI:10.1016/j.engfracmech.2019.106595.
33. Li S, Wang M, Jeanmeure L et al. Damage related material constants in continuum damage mechanics for unidirectional composites with matrix cracks. *International Journal of Damage Mechanics* 2019; 28(5): 690–707. DOI:10.1177/1056789518783239.
34. ROSEN BW. Tensile failure of fibrous composites. *AIAA Journal* 1964; 2(11): 1985–1991. DOI:10.2514/3.2699.

35. Curtin WA. Theory of Mechanical Properties of Ceramic-Matrix Composites. *Journal of the American Ceramic Society* 1991; 74(11): 2837–2845. DOI:10.1111/j.1151-2916.1991.tb06852.x.
36. Neumeister JM. A constitutive law for continuous fiber reinforced brittle matrix composites with fiber fragmentation and stress recovery. *Journal of the Mechanics and Physics of Solids* 1993; 41(8): 1383–1404. DOI:10.1016/0022-5096(93)90085-T.
37. Curtin WA. Exact theory of fibre fragmentation in a single-filament composite. *Journal of Materials Science* 1991; 26(19): 5239–5253. DOI:10.1007/BF01143218.
38. Hui CY, Phoenix S, Ibnabdeljalil M et al. An exact closed form solution for fragmentation of Weibull fibers in a single filament composite with applications to fiber-reinforced ceramics. *Journal of the Mechanics and Physics of Solids* 1995; 43(10): 1551–1585. DOI:10.1016/0022-5096(95)00045-K.
39. Ibnabdeljalil M and Curtin W. Strength and reliability of fiber-reinforced composites: Localized load-sharing and associated size effects. *International Journal of Solids and Structures* 1997; 34(21): 2649–2668. DOI:10.1016/S0020-7683(96)00179-5.
40. Yoshimura A, Okabe T, Yamada M et al. Damage simulation of CFRP laminates under high velocity projectile impact. In *18th International Conference on Composites Materials*. Jeju, South Korea.
41. Maimí P, Camanho P, Mayugo J et al. A continuum damage model for composite laminates: Part I - Constitutive model. *Mechanics of Materials* 2007; 39(10): 897–908. DOI:10.1016/j.mechmat.2007.03.005.
42. Fikry MM, Ogihara S and Vinogradov V. The effect of matrix cracking on mechanical properties in FRP laminates. *Mechanics of Advanced Materials and Modern Processes* 2018; 4(1): 3. DOI:10.1186/s40759-018-0036-6.
43. Okabe T, Sekine H, Ishii K et al. Numerical method for failure simulation of unidirectional fiber-reinforced composites with spring element model. *Composites Science and Technology* 2005; 65(6): 921–933. DOI:10.1016/j.compscitech.2004.10.030.
44. Yamamoto G, Onodera M, Koizumi K et al. Considering the stress concentration of fiber surfaces in the prediction of the tensile strength of unidirectional carbon fiber-reinforced plastic composites. *Composites Part A: Applied Science and Manufacturing* 2019; 121(April): 499–509. DOI:10.1016/j.compositesa.2019.04.011.
45. Okabe T, Imamura H, Sato Y et al. Experimental and numerical studies of initial cracking in CFRP cross-ply laminates. *Composites Part A: Applied Science and Manufacturing* 2015; 68: 81–89. DOI:10.1016/j.compositesa.2014.09.020.
46. Kumagai Y, Onodera S, Salviato M et al. Multiscale analysis and experimental validation of crack initiation in quasi-isotropic laminates. *International Journal of Solids and Structures* 2020; DOI:10.1016/j.ijsolstr.2020.02.010.
47. Kravchenko OG, Kravchenko SG and Pipes RB. Cure history dependence of residual deformation in a thermosetting laminate. *Composites Part A: Applied Science and Manufacturing* 2017; 99: 186–197. DOI:10.1016/j.compositesa.2017.04.006.
48. Malik SA. *Damage detection using self-sensing composites*. Ph. d. thesis, University of Birmingham, 2011.

49. Zhao FM, Okabe T and Takeda N. The estimation of statistical fiber strength by fragmentation tests of single-fiber composites. *Composites Science and Technology* 2000; 60(10): 1965–1974. DOI:10.1016/S0266-3538(00)00084-1.
50. Okabe T, Sekine H, Noda J et al. Characterization of tensile damage and strength in GFRP cross-ply laminates. *Materials Science and Engineering A* 2004; 383(2): 381–389. DOI: 10.1016/j.msea.2004.05.060.